Critical exponents of the fully frustrated two-dimensional XY model

G. Ramirez-Santiago
Department of Physics, Northeastern University, Boston, Massachusetts 02115
and Instituto de Física, Universidad Nacional Autónoma de México, Apartado Postal 20-364, 01000 México, Distrito Federal, Mexico

Jorge V. José
Department of Physics, Northeastern University, Boston, Massachusetts 02115
and Instituut voor Theoretische Fysica, Universiteit Utrecht, Princentonplein 5, Postbus 80.006, 3508 TA Utrecht, The Netherlands
(Received 10 September 1993; revised manuscript received 28 December 1993)

We present a detailed study of the critical properties of the two-dimensional (2D) XY model with maximal frustration in a square lattice. We use extensive Monte Carlo simulations to study the thermodynamics of the spin and chiral degrees of freedom, concentrating on their correlation functions. The gauge-invariant spin-spin correlation functions are calculated close to the critical point for lattice sizes up to 240×240; the chiral correlation functions are studied on lattices up to 96×96. We find that the critical exponents of the spin-phase transition are $\nu=0.3069$ and $\eta=0.1915$, which are to be compared with the unfrustrated XY model exponents $\nu=\frac{1}{2}$ and $\eta=0.25$. We also find that the critical exponents of the chiral transition are $\nu_\chi=0.875$, $2\beta=0.1936$, $2\gamma=1.82$, and $2\gamma'=1.025$, which are different from the expected 2D Ising critical exponents. The spin-phase transition occurs at $T_{U(1)}=0.446$, which is about 7% above the estimated chiral critical temperature $T_{Z_2}=0.4206$. However, because of the size of the statistical errors, it is difficult to decide with certainty whether the transitions occur at the same or at slightly different temperatures. Finally, the jump in the helicity modulus in the fully frustrated system is found to be about 23% below the unfrustrated universal value. The most important consequence of these results is that the fully frustrated XY model appears to be in a novel universality class. Recent successful comparisons of some of these results with experimental data are also briefly discussed.

I. INTRODUCTION

The critical behavior of the uniformly frustrated two-dimensional (2D) XY model has been studied extensively in recent years, both theoretically[1–25] and experimentally.[26–32] This theoretical interest has been due to the rich variety of possible novel critical phenomena that can appear in this model depending on the frustration parameter $f=p/q$, with p and q relative primes. Experimentally, an understanding of the phase transition(s) that occurs in this model is important to describe the physics of two-dimensional periodic arrays of Josephson junctions,[26–32] and two-dimensional superconducting wire networks,[33–34] both in the presence of frustration $f=\Phi/\Phi_0$. Here Φ is the average flux per plaquette normalized to the superconducting quantum of flux $\Phi_0=h/2e$. These arrays can be manufactured with high precision using model photolithographic techniques. Of particular interest is the $f=\frac{1}{2}$ fully frustrated 2D XY model (FFXYM). This model has a continuous U(1) Abelian symmetry, and a discrete Z_2 symmetry leading to the possibility of true long-range order in two dimensions. In contrast, the unfrustrated 2D XY model (XYM) only possesses a continuous U(1) Abelian symmetry: its low-temperature phase is characterized by quasi-long-range order rather than true long-range order.[35–38] In spite of the many experimental and theoretical studies of the FFXYM, there are several questions that remain to be resolved. For example, it is not clear whether one phase transition exists at the critical temperature T_c, which is a combination of a Berezinskii-Kosterlitz-Thouless- (BKT) type transition for the U(1) symmetry plus an Ising-like transition for the Z_2 symmetry, or whether there are two successive phase transitions at critical temperatures $T_{U(1)}$ and T_{Z_2}. Even the order in which they may occur is controversial. More importantly the nature of the transitions, as characterized by their critical properties, is not yet fully understood.

In their original work Teitel and Jayaprakash suggested[4] that in a square lattice the two transitions occurred very close in temperature. They carried out Monte Carlo (MC) simulations to calculate the helicity modulus Υ and the specific heat C as a function of temperature and lattice sizes $L\times L$, with L up to $L=32$. They found that the maximum of the specific heat appeared to increase as $\ln L$, characteristic of a 2D Ising-like transition. Related studies in the triangular lattice antiferromagnetic XYM, which could be expected to be in the same universality class as the FFXYM, indicate that there is a combination of BKT and Ising-like transitions.[6] In Ref. 6, the two transitions appear to take place at the same T_c while in Ref. 7 they are within 2% of each other, with $T_{Z_2}>T_{U(1)}$. In another investigation Berge *et al.*[14] introduced a frustrated XYM with variable frustration on a square lattice. In this model the couplings along the columns are chosen with strength J, while those along every other row have strength $-\mu J$, with $0<\mu\leq1$. From a MC analysis of the specific heat they surmised

that for $\mu < 1$ the model has separate Ising and BKT ordering with $T_{Z_2} < T_{U(1)}$, while for the FFXYM ($\mu = 1$) the two transitions appear to merge into one. The Berge *et al.* model was studied in detail by Eikmans *et al.*[16] who carried out MC calculations of the helicity modulus, which is more sensitive to possible BKT-like ordering, and interpreted their results using a Coulomb gas picture. In another thermodynamic MC study of the related uniformly frustrated square lattice 2D Coulomb gas model, Grest[17] carried out simulations for frustrations $f=0$, $\frac{1}{2}$, $\frac{1}{3}$, and $\frac{1}{4}$ and with L up to 50. He found that in the fully frustrated case the jump in the inverse dielectric constant ϵ_0^{-1} is different from the XYM case. Specifically, the jump in ϵ_0^{-1} occurs at $T_{CG}=0.129\pm0.002$ and takes the value $\epsilon_0^{-1}=0.63\pm0.03$, which is larger than the XYM universal value of 0.52, and agrees with Minnhagen's conjecture.[39] The determination of the jump was based, however, on the criterion used for the XYM. Grest found, as in previous studies, that the specific heat grows logarithmically with L. It is significant that his results appear to indicate a clear separation of the two critical temperatures with $T_{Z_2} > T_{U(1)}$, contrary to previous conjectures.

Granato *et al.*[19] have studied the Z_2 critical behavior of a coupled XY-Ising system using MC and MC transfer-matrix calculations. An important finding in this study is the chiral critical exponent $\nu_\chi \sim 0.85(3)$, which is clearly different from the 2D Ising model value of $\nu=1$.[18] Furthermore, they found that the XY and Ising transitions occur at essentially the same temperature. Lee, Kosterlitz, and Granato[20] carried out MC simulations of the FFXYM in the square and triangular lattices and found that ν is also different from the 2D Ising model result.

In the XYM the nature of the BKT phase is characterized by the approximate analytic expression for the spin-spin correlation functions.[36,37] However, unlike in the XYM case, it has proven to be very difficult to calculate the correlation functions for the FFXYM analytically. This difficulty exists partly because in order to carry out the calculations one needs to include the basic excitations of the frustrated problem, which consist of different types of fractional charges as well as the Ising model related domain walls.[11] Nonetheless, it has been possible to extract some qualitative information about the critical properties using techniques such as the renormalization-group approximation[9] applied to an effective Hamiltonian obtained from a Hubbard-Stratonivich transformation of the FFXYM (Ref. 8) or by general symmetry arguments.[10] One worry about the effective Hamiltonian is that it does not explicitly contain the same elementary excitations as the original FFXYM, such as the fractional charges. All of the studies mentioned above have mostly concentrated on calculating thermodynamic quantities, for it has been difficult to separate the Z_2 from the U(1) contributions.

The purpose of this paper is to fill this gap by explicitly calculating the U(1) and Z_2 correlation functions as well as the separate Z_2 contribution to the magnetic properties. We should mention at the outset that these calculations are significantly more demanding than the thermodynamic calculations and are now possible because of improved algorithms and computer power. One further complication is that at present there is no available analytic theory for the $f \neq 0$ case that could suggest what form these correlation functions should have and we need to make an *ansatz* for them. Generally, we can either assume that they decay exponentially or algebraically with distance. We use different statistical measures to test for the two possibilities. If our MC results for the correlation functions are consistent with an exponential decay we extract a correlation length $\xi(T)$, while if they are consistent with a power-law decay we extract the corresponding $\eta(T)$ exponent. In the case that $\xi(T)$ diverges at T_c from above it can diverge as a power law or with the BKT form $\sim\exp[B(T-T_c)^{-\nu}]$. In the $f=0$ case the critical exponent $\nu(f=0)=1/2$.[36,37] In the low-temperature phase of the XYM the correlation function decays algebraically with distance r as $\sim r^{-\eta}$, where the η exponent is a continuous function of T and takes the universal value $\eta(f=0,T_{BKT})=\frac{1}{4}$. Several experiments have confirmed the $f=0$ picture and the values of the measured critical exponents[40–42] agree well with those predicted by theory. In addition, recent MC simulations have provided an accurate evaluation of the $f=0$ XYM critical exponents.[43–47] The most recent[46] high-statistics estimates for $f=0$ are $\nu=0.4695(1)$ and $\eta=0.235$, with the critical temperature $T_{BKT}=0.8953$.

In order to understand the nature of the phase transitions in the FFXYM we have studied a variety of quantities, several of which separately describe each particular symmetry. The thermodynamic quantities calculated are the helicity modulus, Υ, and the square of both the staggered chiral magnetization, $\mathcal{M}_s^2$, and susceptibility, χ_s^2. We have carried out an extensive analysis of the gauge-invariant U(1) correlation function, $g_{U(1)}(r)$ and their corresponding even and odd coherence lengths (to be defined below). These calculations have allowed us to extract the U(1) critical temperature, $T_{U(1)}$, and its critical exponents ν and η. For the Z_2 freedoms we calculated the chiral correlation function, $g_\chi(r)$, and its corresponding coherence length, ξ_χ, which allowed us to estimate the critical exponent ν_χ and the critical temperature T_{Z_2}. Our result for the exponent ν_χ is in very good agreement with the recent MC transfer-matrix calculation.[25]

We will now outline the main results of our study. Our extensive analysis is consistent with a U(1) BKT-type transition but with exponents $\nu(f=\frac{1}{2})=0.3069$ and $\eta(f=\frac{1}{2},T_c)=0.1915$. These results clearly differ from those obtained in the XYM case.[36,37,43] We have also calculated the Z_2 critical exponent $2\beta=0.1936(35)$ for $\mathcal{M}_s^2$, $2\gamma=1.82(13)$ and $2\gamma'=1.025(79)$ for χ_s^2, and the coherence length exponent $\nu_\chi=0.875$. These exponents are also different from those expected for a 2D Ising model. The critical temperatures found in our study are $T_{U(1)}=0.446$ and $T_{Z_2}=0.4206$. One could be tempted to say that the transitions take place at two different temperatures, and this may indeed be the case. However, after a detailed assessment of the size of the statistical er-

rors from the nonlinear fits and considering the small difference between the two temperatures we cannot be certain if they are different or not. Furthermore, the transitions are reversed from their expected order. We suspect that more extensive simulations with algorithm improvements, better statistics, and larger system sizes are needed to clarify this point. The results mentioned above were obtained from extensive MC simulations on a square lattice of size L, with L ranging from $L=8$ up to 240, and with periodic boundary conditions. What emerges from our results is that the FFXYM is in a novel universality class different from either a pure XY or an Ising universality class. A brief description of some of the results presented here has appeared elsewhere.[22]

We have also recently reanalyzed the experimental results of the Delft group[48] for $f=0$ and $\frac{1}{2}$. We have concluded that the values of $\eta(f=0)=\frac{1}{4}$ and $\eta(f=\frac{1}{2})=0.1915\approx\frac{1}{5}$ are in good agreement with the experimental data. However, the fits of the experimental resistance versus temperature data cannot distinguish between a $\nu(f=\frac{1}{2})=\frac{1}{3}$ from a $\nu(f=\frac{1}{2})=\frac{1}{2}$. Moreover, as mentioned above, recent MC transfer-matrix work has provided further evidence that the chiral exponents are not equal to the 2D Ising model exponents and even quantitatively the value of ν_χ has begun to converge on values close to 0.85.

The organization of this paper is as follows: In Sec. II A, we define and briefly review the general properties of the uniformly frustrated 2D XYM. In Sec. II B, we define the thermodynamic quantities calculated in this paper, while in Sec. II C we give the expressions for the calculated gauge-invariant U(1) and Z_2 zero-momentum correlation functions, of central interest here, together with their possible asymptotic behaviors. In Sec. III A, we describe briefly the MC algorithm used in our calculations. Since there are no analytic results for the correlation functions to guide our analysis, we proceed by developing an approach that consists of using several independent checks of the results obtained. As a test, in Sec. III B, we successfully apply our strategy to the unfrustrated XYM and compare our results to those obtained in the more extensive recent MC studies.[43–46] In Sec. IV, we present the bulk of our numerical MC results applied to the FFXYM. In Sec. IV A, we discuss the thermodynamic results for both the U(1) and Z_2 freedoms. In Sec. IV B 1, we give the correlation function results for the U(1) freedoms, including a finite-size scaling analysis for the correlation length. In Sec. IV C 2 we present the corresponding correlation function results for the Z_2 freedoms. Finally, in Sec. V, we present a critique of our results and a possible outlook for the future.

II. THE FULLY FRUSTRATED XY MODEL

A. Definition of the model

The uniformly frustrated 2D XYM is defined by the Hamiltonian

$$H=-\sum_{\langle \mathbf{r},\mathbf{r}'\rangle} J\cos[\theta(\mathbf{r})-\theta(\mathbf{r}')+f(\mathbf{r},\mathbf{r}')]\ , \tag{1}$$

where $\theta(\mathbf{r})$ is the angle at site $\mathbf{r}$, $\langle \mathbf{r},\mathbf{r}'\rangle$ stands for a sum over nearest-neighbor lattice sites, and J is the exchange constant. In the Josephson junction array representation of the model in a transverse magnetic field, the bond variables $f(\mathbf{r},\mathbf{r}')$ are given by the line integral $f(\mathbf{r},\mathbf{r}')=(2\pi/\Phi_0)\int_{\mathbf{r}}^{\mathbf{r}'}\mathbf{A}\cdot d\mathbf{l}$, with $\mathbf{A}$ the magnetic vector potential. For uniform frustration these bond angles are required to satisfy

$$\sum_{\text{plaquette}} f(\mathbf{r},\mathbf{r}')=\frac{2\pi}{\Phi_0}\oint_{\text{plaquette}}\mathbf{A}\cdot d\mathbf{l}=2\pi f\ . \tag{2}$$

The Hamiltonian defined in Eq. (1) is invariant under the transformation, $\theta(\mathbf{r})\rightarrow\theta(\mathbf{r})+2\pi n(\mathbf{r})$ and

$$f(\mathbf{r},\mathbf{r}')\rightarrow f(\mathbf{r},\mathbf{r}')+2\pi[n(\mathbf{r}')-n(\mathbf{r})]\ ,$$

where $n(\mathbf{r})$ and $n(\mathbf{r}')$ are integer numbers. Choosing the gauge $\mathbf{A}=(-By,0,0)$ so that $\mathbf{B}=B\hat{\mathbf{z}}$ and assuming a square lattice, the bond angles $f(\mathbf{r},\mathbf{r}')$ are given by

$$f(\mathbf{r},\mathbf{r}')=\mp 2\pi f(j+\tfrac{1}{2}) \quad \text{for } \mathbf{r}'=\mathbf{r}\pm a_0\mathbf{i} \tag{3a}$$

and

$$f(\mathbf{r},\mathbf{r}')=0 \quad \text{for } \mathbf{r}'=\mathbf{r}\pm a_0\mathbf{j}\ . \tag{3b}$$

Here $f=Ba_0^2/\Phi_0$ with $\mathbf{r}=(ia_0,ja_0)$, i,j integers, and a_0 the lattice spacing. The uniformly frustrated model is periodic in f with period one, and with reflection symmetry about $f=\frac{1}{2}$. The XYM corresponds to the unfrustrated $f=0$ case.

The fully frustrated case corresponds to $f=\frac{1}{2}$. The effect of f in this case is to produce alternate rows with ferro- and antiferromagnetic couplings, while the couplings along the columns are all ferromagnetic. Each plaquette has one antiferromagnetic and three ferromagnetic bonds, or vice versa, leading to a ground state that has a twofold degeneracy with half-integer vortices of opposite circulation or chirality.[1] Thus, the system displays two symmetries: the underlying continuous U(1) Abelian symmetry for the phases and a discrete Z_2 or Ising-like symmetry associated with the chiral degrees of freedom.

B. Thermodynamic properties

The helicity modulus Υ is defined by the response of the system to a twist in the spins at its boundaries. In our case Υ is calculated explicitly from the formula

$$\Upsilon=\frac{1}{N}\left[\left\langle\sum_{\langle \mathbf{r},\mathbf{r}'\rangle} x_{\mathbf{r},\mathbf{r}'}^2\cos[\theta(\mathbf{r})-\theta(\mathbf{r}')+f(\mathbf{r},\mathbf{r}')]\right\rangle-\frac{1}{k_BT}\left\langle\left[\sum_{\langle \mathbf{r},\mathbf{r}'\rangle} x_{\mathbf{r},\mathbf{r}'}\sin[\theta(\mathbf{r})-\theta(\mathbf{r}')+f(\mathbf{r},\mathbf{r}')]\right]^2\right\rangle\right.$$
$$\left.+\frac{1}{k_BT}\left[\left\langle\sum_{\langle \mathbf{r},\mathbf{r}'\rangle} x_{\mathbf{r},\mathbf{r}'}\sin[\theta(\mathbf{r})-\theta(\mathbf{r}')+f(\mathbf{r},\mathbf{r}')]\right\rangle^2\right]\right]\ , \tag{4}$$

where $\langle\ \rangle$ stands for a thermal average, and k_B is Boltzmann's constant, and $x_{r,r'}=x_r-x_{r'}$. Another informative quantity associated with the supercurrent loops around a plaquette in a Josephson array is the staggered magnetization

$$M_{\text{stagg}}=\frac{1}{N}\left\langle \sum_{\mathcal{P}(\mathbf{R})}(-1)^{R_x+R_y}\left[\sum_{\langle \mathbf{r},\mathbf{r}'\rangle\in\mathcal{P}(\mathbf{R})}\sin[\theta(\mathbf{r})-\theta(\mathbf{r}')+f(\mathbf{r},\mathbf{r}')]\right]\right\rangle , \tag{5}$$

where (R_x,R_y) give the coordinates at the center of the plaquette $\mathcal{P}$. The index $\mathcal{P}(\mathbf{R})$ runs from 1 up to N, the total number of plaquettes in the lattice.

We now turn to the definition of the quantities associated with the chiral degrees of freedom. The *chirality* of a plaquette gives the direction of circulation of the supercurrents induced by frustration. Each plaquette has a definite *chirality* which can be ± 1, and it is calculated from[1]

$$\chi(\mathbf{R})=\text{sgn}\left[\sum_{\langle \mathbf{r},\mathbf{r}'\rangle\in\mathcal{P}(\mathbf{R})}\sin[\theta(\mathbf{r})-\theta(\mathbf{r}')+f(\mathbf{r},\mathbf{r}')]\right] , \tag{6}$$

with the dual lattice vector $\mathbf{R}=[(i+1/2)a_0,(j+1/2)a_0]$ with i,j integer numbers. At zero temperature the chiralities are ordered like a 2D Ising antiferromagnet. At finite temperatures there are line or domain-wall defects separating regions with different chiralities.

The order parameter describing the Z_2 phase transition is the *staggered chiral magnetization,* defined by

$$\mathcal{M}_s=\left\langle \frac{1}{N}\sum_{\mathbf{R}}(-1)^{R_x+R_y}\chi(\mathbf{R})\right\rangle . \tag{7}$$

It is difficult to study this quantity numerically since it oscillates rapidly between positive and negative values. A more stable quantity to study is Binder's second-order cumulant, $\mathcal{M}_s^2$ and its fluctuations.[7] These fluctuations are given by the square of the *staggered chiral susceptibility,* calculated as

$$\chi_s^2=N\left\langle \frac{\Delta\mathcal{M}_s^2}{k_BT}\right\rangle . \tag{8}$$

Our numerical results for the thermodynamic quantities characterizing the chiral degrees of freedom will be presented in Sec. IV A 2. It will be seen that close to the critical region their behavior is quantitatively different from an Ising ferromagnet on a square lattice.

C. Correlation functions

It is known that the hallmarks of the BKT ordering can be given in terms of the phase correlation functions. An analytic evaluation of these quantities appears to be mathematically intractable for uniform frustration. Nonetheless, for random frustration it has been possible to analytically calculate the correlation functions at low temperatures in the limits where the density x_f of frustrated plaquettes[3] is $x_f\ll 1$ or $x_f\sim\frac{1}{2}$. Given that the Hamiltonian of the frustrated XYM is gauge invariant, the phase correlation functions should also be gauge invariant. The correlation functions are defined along a path connecting the correlated spins and are therefore path dependent. In fact, gauge-invariant correlation functions along two different paths differ by the total amount of frustration enclosed by the two paths. The gauge-invariant phase correlation function along a path Γ that accounts for the frustration in the system is given by[2,3]

$$g_{\text{U(1)}}(\mathbf{r},\mathbf{r}')=\left\langle e^{i\theta(\mathbf{r})}\left[\prod_{\langle \mathbf{s},\mathbf{s}'\rangle\in\Gamma}e^{if(\mathbf{s},\mathbf{s}')}\right]e^{-i\theta(\mathbf{r}')}\right\rangle . \tag{9}$$

In Fig. 1, we show two possible trajectories $\Gamma_A(\mathbf{r},\mathbf{r}')$ and $\Gamma_B(\mathbf{r},\mathbf{r}')$ joining the points $\mathbf{r}$ and $\mathbf{r}'$. The phase introduced in Eq. (9) when going around the trajectory A is

$$\prod_{\Gamma_A}e^{if(\mathbf{s},\mathbf{s}')}=\exp\left[\sum_{\Gamma_A}f(\mathbf{s},\mathbf{s}')\right] ,$$

while if one follows trajectory B the phase factor is given by

$$\prod_{\Gamma_B}e^{if(\mathbf{s},\mathbf{s}')}=\exp\left[\sum_{\Gamma_B}f(\mathbf{s},\mathbf{s}')\right] .$$

The total frustration contained in the area enclosed by both trajectories is then

$$\sum_{\langle \mathbf{s},\mathbf{s}'\rangle\in\Gamma_A}f(\mathbf{s},\mathbf{s}')+\sum_{\langle \mathbf{s},\mathbf{s}'\rangle\in\Gamma_B}f(\mathbf{s},\mathbf{s}')=2\pi Mf , \tag{10}$$

where M represents the number of elementary plaquettes inside the area encircled by the paths, and f is the frustration of each plaquette. In this case the phase in Eq. (9) is shifted by an additional amount $2\pi Mf$ when the correlation along trajectory B is calculated instead of A.

To evaluate the effect of frustration on the correlation functions at low temperatures one can use duality transformations to obtain a lattice Coulomb gas representation of the model.

After doing so one obtains[3]

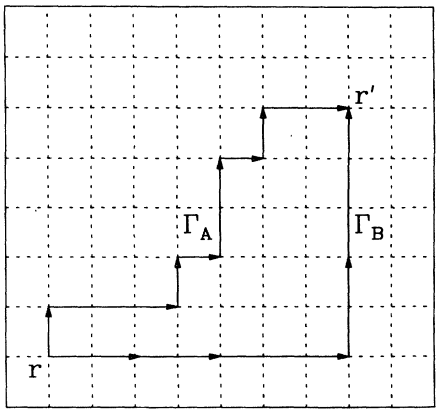

FIG. 1. Possible trajectories $\Gamma_A(\mathbf{r},\mathbf{r}')$ and $\Gamma_B(\mathbf{r},\mathbf{r}')$ used in evaluating $g_{\text{U(1)}}(\mathbf{r},\mathbf{r}',\Gamma_A)$ and $g_{\text{U(1)}}(\mathbf{r},\mathbf{r}',\Gamma_B)$.

$$g_{U(1)}(\mathbf{r},\mathbf{r}')=\exp\left[i\sum_{\mathbf{r}}\sum_{\mathbf{R}}\tfrac{1}{2}n(\mathbf{r})\Theta(\mathbf{r}-\mathbf{R})f(\mathbf{R})\right]g_{CG}(\mathbf{r},\mathbf{r}')\ , \tag{11}$$

where $g_{CG}(\mathbf{r},\mathbf{r}')$ is the lattice Coulomb gas correlation function for the XYM (Ref. 37) and $f(\mathbf{R})$ is the frustration at the plaquette with center at the dual lattice site $\mathbf{R}$. The number $n(\mathbf{r})$ is zero everywhere, except at $\mathbf{r}$ and $\mathbf{r}'$, where it takes the values $n(\mathbf{r})=-n(\mathbf{r}')=1$.[3] The angular potential $\Theta(\mathbf{R})$ is given by[37] $i\Theta(z)=\ln(z)-G(|z|)$, for large R. Here $z=R_x+iR_y$ and $\mathbf{R}=(R_x,R_y)$. Notice that in Eq. (11) there is an extra phase factor appearing in the phase correlation function. This factor weights the contributions to the correlation function coming from different trajectories going between r and r', and it is a consequence of gauge invariance or, equivalently, the Aharanov-Bohm effect. We shall see that this extra phase factor in the correlation function appears naturally in the results discussed in Sec. IV A 1.

In the evaluation of the correlation functions we can have important contributions from more than one Lyapunov exponent, which makes the extraction of the largest exponent difficult. However, this problem is not present if we evaluate the zero-momentum correlation function defined by[43]

$$g_0(r)=\langle \mathbf{S}_{av}(i)\cdot\mathbf{S}_{av}(i+r)\rangle\ , \tag{12}$$

where

$$\mathbf{S}_{av}(i)=\frac{1}{L_y}\sum_j \mathbf{S}(i,j) \tag{13}$$

is the average spin along the ith column. In this case r denotes the distance between the columns being correlated.

From the definition of the gauge-invariant phase correlation function, Eq. (9), the expression for the zero-momentum correlation function is

$$g_{U(1)}(r)=\left\langle \frac{1}{L_xL_y}\sum_{j=1}^{L_y}\sum_{i=1}^{L_x}\cos[\theta_{i+r,j}-\theta_{i,j}+\pi(j+\tfrac{1}{2})r]\right\rangle\ , \tag{14}$$

where we have used Eqs. (3).

A similar reasoning applies to the zero-momentum chiral correlation function given by

$$g_\chi(r)=\left\langle \frac{1}{L_xL_y}\sum_{i=1}^{L_x-1}\sum_{j=1}^{L_y-1}\chi_{i+r,j}\chi_{i,j}\right\rangle\ . \tag{15}$$

We have used Eqs. (14) and (15) to evaluate the correlation functions in our numerical simulation.

As mentioned before there are no known explicit analytic expressions for $g_{U(1)}(r)$ and $g_\chi(r)$. Nonetheless, we can make an *ansatz* for the analytic form of these correlations close to the critical region. Our *ansatz* is based on what is known about the XYM and about general properties of standard second-order phase transitions. In the XYM as $T\to T_{BKT}^{+}$ the asymptotic form of the spin-spin correlation function for $r\gg 1$ is

$$g_0(r)=\frac{\mathcal{A}_0}{r^{\eta_0}}\times e^{-r/\xi_0}\ , \tag{16}$$

with $n_0=\frac{1}{4}$ and the coherence length diverging as

$$\xi_0(T)=A_0\exp\left[\frac{B_0}{(T-T_{BKT})^{\nu_0}}\right]\ . \tag{17}$$

In the XYM the critical exponent $\nu_0=1/2$.[36] In the low-temperature phase ($T\le T_{BKT}$) the long-distance correlation function decays as

$$g_0(r)=\frac{C_0}{r^{\eta_0(T)}}\ . \tag{18}$$

The exponent η_0 is a function of temperature, representing a continuous line of critical points. In the XYM η_0 takes the universal value $\eta_0(T=T_{BKT})=\frac{1}{4}$.[36,37] This result is directly related to the universal jump predicted for the superfluid density.[38]

In the disordered phase of the 2D Ising model ($T>T_I$), the asymptotic behavior of the correlation function close to T_I is given by[49]

$$g_I(r)=\frac{A_I}{r^{\eta_I}}\times e^{-r/\xi_I} \tag{19}$$

again with $\eta_I=\frac{1}{4}$ and with a power-law divergence for the coherence length

$$\xi_I(T)=\frac{A_I}{(T-T_I)^{\nu_i}}\ , \tag{20}$$

where the critical exponent $\nu_I=1$. In the ordered phase ($T\le T_I$), the asymptotic behavior of the correlation functions is given by[49]

$$g_I(r)=\frac{C_I}{r^{\eta_I}}\times e^{-r/\xi_I}+\langle M_I\rangle^2\ , \tag{21}$$

valid for $\epsilon_I=(T_I-T)/T_I\ll 1$ and $\epsilon_I r<1$. The correlation function critical exponent at T_I is $\eta_I=\frac{1}{4}$, as in the XYM.

Based on previous studies of the thermodynamics of the FFXYM it is reasonable to assume that their asymptotic behavior for $f=\frac{1}{2}$ can be described by either BKT or Ising-like forms described above. In our calculations we checked for the best fits to our MC data by either form.

Having discussed the expected analytic forms for the different correlation functions of interest, let us now turn to a discussion of their numerical evaluation. We should notice first that, strictly speaking, for finite lattices the asymptotic behavior of the correlation functions is not accessible. Even in rather large lattices the subleading power-law behavior of the correlation functions can be non-negligible. Thus, the evaluation of the coherence length extracted from a numerical calculation of the correlation function is nontrivial. A common procedure is to take periodic boundary conditions and then fit the behavior of the correlations to

$$G(r)=g(r)+g(L-r)\ , \tag{22}$$

where $g(r)$ is any of the correlation functions of interest. We should note that, in general, it is not sufficient to account for the closest images to the source along the r direction but we must also account for the images farther away as well as those in the direction transverse to r. In fact, their contribution becomes more important as the coherence length ξ grows since the number of relevant images increases.

III. CALCULATIONAL STRATEGY AND TEST

Our strategy is to carry out several independent consistency checks of our results, for there are no analytic result with which to guide the analysis. To test the reliability of our consistency checks, we start by applying them to the extensively studied XYM. Although there is a basic consensus about the physical nature of the BKT transition, relatively reliable and thorough nonperturbative numerical studies of the critical exponents of the XYM became available just recently.[43–47] Here we tried to follow some of the basic ideas of these approaches, in particular the one used above T_c, complemented with other tests implemented here. We must stress that we are on less firm ground in the FFXYM case than in the XYM and thus we need extra consistency checks that were not needed in the XYM studies.

A. MC algorithm

Different acceleration algorithms that have worked out well in the XYM were constructed with special regard to the nature of the basic excitations in the model. In the FFXYM we have a less definitive idea about the basic excitations in the model and therefore the same type of algorithms have not proven any more efficient than the standard Metropolis approach.[49,50] Our simulations were then carried out using the standard Metropolis algorithm in square lattices of sizes $L\times L$ with $L=8$, 16, 32, 60, 72, 84, 96, 180, and 240, with periodic boundary conditions. The lattice sizes $L=120$ and $L=180,240$ were considered only at two temperatures that are about 3 and 2% away from the estimated critical point, respectively. These relatively large lattices were studied in order to get a better estimate of the U(1) correlation function critical exponents. For the thermodynamic and chiral degrees of freedom a full set of temperature values was considered for L up to $L=84$. Since we expect to have critical slowing down similar to that seen in the XYM, which has decorrelation times growing as ξ^2, we performed reasonably long runs, although no detailed attempt was made to calculate the FFXYM dynamic critical exponent. Nonetheless, our consistency and self-consistency checks give support to the reliability of our results. The equilibration time of a typical run was at least 10 K MCS/angle far from criticality and at least twice as much for temperatures close to T_c. The statistics were calculated from runs of at least 50 K MCS/angle, and up to 290 K MCS/angle. Details of the length of the runs are given in the tables. It is important to note here that since we are interested in extracting critical exponents from nonlinear fits, plots of the results are sometimes not as informative as looking at the numbers themselves.

B. Unfrustrated 2D XY model

We begin by presenting our results for the XYM together with the tests of our consistency checks for both Υ^0 and the correlation functions. We compare our XYM results to those obtained recently by more extensive analysis.[46] In the next section we shall present the bulk of the results of our calculations with the FFXYM. Note that in terms of the correlation functions the difficult calculations are those for the U(1) symmetry, for in that case the correlation length may diverge exponentially rather than algebraically as one gets close to T_c.

We now describe the numerical approach to calculate the coherence length, the critical temperature and critical exponents from the U(1) correlation functions. We have to some extent repeated the recent, more extensive calculations for the XYM (Refs. 43–46) critical exponents for $T>T_{\rm BKT}$, and we have extended the calculations to the $T\le T_{\rm BKT}$ region. To facilitate the comparison of our results, given in Table I (top), to previous findings we have summarized the results of Refs. 43–46 in Table I (middle) and (bottom). Basically, we have followed the method of analysis used in those references, although the lattices we

TABLE I. Critical exponents and critical temperatures for the XYM. (Top) In the first and second columns we give the results obtained from fitting the $T>T_{\rm BKT}$ ξ_0 data to Eqs. (17) and (20), respectively. The third column gives the parameters obtained from an algebraic fit to $g_0(r)$ at $T=T_{\rm BKT}$. (Middle) Same as in (top) for the first two columns with results from Ref. 46, obtained from unconstrained four-parameter nonlinear fits. (Bottom) The first two lines are the η_0 exponents obtained from a high-temperature analysis of the susceptibility, χ (from Ref. 44). The third and fourth lines give η_0 obtained from MC renormalization-group calculations (Ref. 46).

$T>T_{\rm BKT}$	$T>T_c$	$T=T_{\rm BKT}$
$\xi=a_0\times\exp[B_0\epsilon_{\rm BKT}^{-\nu_0}]$	$\xi=A_0'\times\epsilon_c^{-\nu_0'}$	$g(r)=C_0/r^{\eta_0}$
$A_0=0.2050$	$A_0'=0.87$	$C_0'=0.7099$
$B_0=1.6113$		
$T_{\rm BKT}=0.9035$	$T_c=0.9797$	
$\nu_0=0.4797$	$\nu_0'=1.0534$	$\eta_0=0.2386$
$\chi^2/{\rm DOF}=0.446$	$\chi^2/{\rm DOF}=0.3523$	$\chi^2/{\rm DOF}=0.00826$
${\rm DOF}=8$	${\rm DOF}=9$	${\rm DOF}=46$

$T>T_{\rm BKT}$	$T>T_c$
$A_0=0.1806$	$A_0'=0.87$
$B_0=1.8727$	
$T_{\rm BKT}=0.8953$	$T_c=0.970$
$\nu_0=0.4695$	$\nu_0'=1.15$
$\chi^2/{\rm DOF}=0.933$	$\chi^2/{\rm DOF}=2.4$
${\rm DOF}=29$	${\rm DOF}=11$
$\chi(T)\vert_{T\to T_{\rm BKT}^+}$	$\chi^2_{\rm DOF}$
$\eta_0=0.287(3)$ $(\xi>5)$	2.05
$\eta_0=0.280(4)$ $(\xi>10)$	2.22
η_0 $(T_{\rm BKT}=0.894)=0.235$	MCRG
$\eta_0^-=0.236$	FSA

have simulated are not as large as the ones considered there. However, to reduce the finite-size effects and to ensure meaningful results for the correlation functions, we kept the ratio $L/\xi_0 \geq 4$ in all the calculations. We note that, even though the critical temperatures in the FFXYM is about $T_{BKT}/2$, we kept this ratio at $L/\xi \geq 5$. The calculational procedure is the following: First, the periodic form of the zero-momentum correlation function $g_0(r)$ given in Eqs. (14) and (22), with $f=0$, was calculated in the high-temperature phase. Next, we carried out unconstrained three-parameter nonlinear fits of the data to the form given in Eq. (16). From these fits we determined $\xi_0(T)$ and the parameters η_0 and A_0. To further check the consistency of the nonlinear fits we performed linear fits to the MC data of the form

$$\ln[g_0(r)]=\ln A_0+\ln[r^{-\eta_0}e^{-r/\xi_0}+(L-r)^{-\eta_0}e^{-(L-r)/\xi_0}] \tag{23}$$

varying the values of η_0 until we reached a minimum for the χ^2 function. We found that $\xi_0(T)$ is systematically above the values of Ref. 43 (for the comparison see Fig. 2), and that $\eta_0(T)$ oscillates nonmonotonically close to the critical point, making its determination difficult. We also carried out an unconstrained four-parameter nonlinear fit to the data to extract T_{BKT} and ν_0, assuming a BKT form for $\xi_0(T)$. As pointed out in a recent finite-size scaling analysis[45] of the XYM susceptibility, it is very difficult to distinguish between a BKT form and a power-law divergence on the basis of data obtained from MC simulations on lattices up to $L=256$, even for temperatures 1% away from the critical point. Thus, we carried out an additional unconstrained three-parameter nonlinear fit to a power-law form [Eq. (20)]. The results of these fits are summarized in the first and second columns of Table I (top). Before proceeding with a discussion of these results, let us emphasize that we carried out a careful analysis of the stability of the parameters obtained from the fits by trying to make sure that the values obtained correspond to the minimum of the χ^2 function, within the statistical errors of our simulations. More details of the fitting procedure and related analyses will be discussed below.

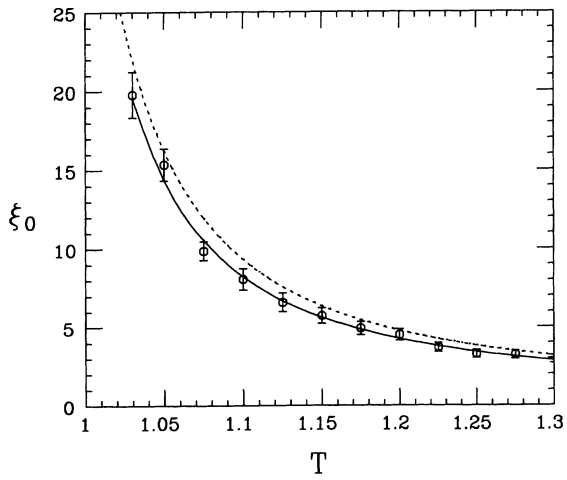

FIG. 2. Correlation length ξ_0 as a function of temperature. The circles denote the results from the fits to the correlation function given in Eq. (16), with their corresponding statistical errors. The solid line is the result of a fit of the data to the expression for $\xi_0(T)$ given in Eq. (17). The specific values of the fitting parameters is given in Table I (top). The dashed line was obtained using the fitted parameters from Ref. 43.

Let us now turn to the results obtained by assuming a BKT form for $\xi_0(T)$. We find that the values of the parameters A_0 and B_0 in the first column of Tables I (top) and (middle) agree well, while the values of ν_0 and T_{BKT} differ by 4 and 0.75 %, respectively. The results obtained assuming a power-law form are given in the second column of Tables I (top) and (middle). The values of T_c and ν_0' are within 1 and 9 %, respectively, whereas the values for the A_0''s are the same. All of these results indicate that there is good agreement between our results and those obtained from the more extensive MC simulations, in spite of the fact that our simulations are in smaller systems and have less statistics. It is important to realize that fitting the coherence length to a BKT or to a power-law form leads to χ^2/DOF values of comparable quality. Thus, from this analysis alone one cannot decide which of the two fits is the correct one. To sort out this problem we also have calculated the low-temperature $g_0(r,T)$. The correlations, for $L=60$ lattices, were fitted to $g_0(r)\sim r^{-\eta_0}$ and

$$g_0(r)\sim[r^{-\eta_0}e^{\alpha_0 r}+(L-r)^{-\eta_0}e^{\alpha_0(L-r)}], \tag{24}$$

at nine different temperatures. The results of these fits are given in Tables II (top) and (second section). It is found that the exponential fits appear to be of better quality, and the corresponding values of $\eta_0(T)$ are systematically above those obtained from the algebraic fits. However, the important point is that the values of the exponents α are smaller than 10^{-2}, suggesting a coherence length too large for the fit to be trusted. Moreover, the algebraic fits agree with the low-T spin-wave prediction, $\eta_0(T)\sim T$. In Fig. 3(a), we show the results for η_0 as a function of temperature. To further analyze the nature of the low-temperature phase, we calculated $\eta_0(T_{BKT})=\eta_{0c}$ as a function of lattice size, using the T_{BKT} obtained at high temperatures and for reasonably long runs. On the other hand, the exponential fits yielded values of η_{0c} systematically above those calculated from the algebraic fit, shown in Fig. 3(b). Fits to the exponential form plus its image lead to better results in this case. We found that the values of α are quite small and it appears that they become smaller as L increases. This suggests that the algebraic contribution will dominate in the asymptotic limit. Notice also that η_0 increases slowly with L and it does not seem to saturate for the larger lattices in both types of fits. The values for the exponents calculated from both types of fits in the largest lattices do agree with those obtained in Refs. 44 and 46, with the later results given in Table I (bottom) for comparison. The value $\eta_0=0.2386(2)$ calculated from our algebraic fits is in very good agreement with MC renormalization-group calculations.[46] However, the value $\eta_0=0.2713(2)$ obtained by assuming an exponential fit plus its images at

$T=T_{BKT}$ also agrees with the results[44] obtained studying the relationship between $\xi_0(T)$ and the susceptibility $\chi(T)$ as $T\to T_{BKT}^{+}$. The results from the present analysis suggest, as expected, that the algebraic form gives a better fit in the low-temperature phase.

As a further check to this conclusion, to be used in the FF*XYM* analysis, we now show that the values of T_{BKT}, Υ^0, and η_0, which were determined independently, are consistent with the universal value for the jump in $\Upsilon^0(T=T_{BKT})$. We calculated the magnitude of the jump in $\Upsilon^0(T=T_{BKT})$, for sizes $L=8$, 16, 24, 32, 48, 60, 72, 84, and 96, and carried out a finite-size analysis. We used the $T_{BKT}=0.9035(6)$ obtained from the high-temperature analysis of the U(1) correlation functions, to be described below. The results are given in Table III (top). We got the extrapolated value of

$$\Upsilon^0(T_{BKT})=0.5986(49) \tag{25}$$

for the infinite system, by fitting a straight line to $\Upsilon^0(T_{BKT})$ versus L^{-1}, and using the $L=48$–96 results [see Fig. 4(a)]. We also estimated the magnitude of the jump from the universal intercept of $\Upsilon^0(T_{BKT})$ with the $2T_{BKT}/\pi$ line getting

TABLE II. (Top) Results from fits to the data for the correlation function $g_0(r)$ to the form given in Eq. (18) for $L=60$. (Second section) L dependence of η_0 and C_0 at $T=T_{BKT}$. (Third section) Results from exponential fits to the data of $g_0(r)$ for $T<T_{BKT}$ for $L=60$. (Bottom) L-dependent results for η_0, α_0, and C_0 from exponential fits to the correlations at $T=T_{BKT}$.

T	η_0	C_0	χ^2/DOF	NMCS (K)
0.903 5	0.199 6	0.667 8	1.27×10^{-2}	250
0.875	0.184 4	0.685 2	1.25×10^{-2}	120
0.850	0.180 8	0.706 2	0.934×10^{-2}	120
0.825	0.150 6	0.696 2	2.3×10^{-2}	120
0.800	0.140 4	0.707 0	2.21×10^{-2}	140
0.750	0.133 6	0.741 0	1.33×10^{-2}	130
0.700	0.132 0	0.776 3	1.06×10^{-2}	130
0.650	0.106 0	0.770 3	2.77×10^{-2}	130
0.600	0.088 8	0.790 0	2.11×10^{-2}	130

L	η_0	C_0	χ^2/DOF	NMCS (K)
40	0.181 6	0.653 2	0.73×10^{-2}	290
48	0.176 1	0.644 9	1.35×10^{-2}	290
60	0.199 6	0.667 8	1.27×10^{-2}	250
72	0.214 7	0.684 0	1.24×10^{-2}	250
84	0.216 8	0.686 6	1.14×10^{-2}	250
96	0.238 6	0.709 9	0.826×10^{-2}	25

T	η_0	α_0	C_0	χ^2/DOF	NMCS (K)
0.903 5	0.280 2	0.006 7	0.743 6	4.02×10^{-4}	250
0.875	0.260 5	0.004 7	0.762 0	1.2×10^{-3}	120
0.850	0.237 7	0.004 4	0.763 1	5.24×10^{-3}	120
0.825	0.224 6	0.006 0	0.770 5	2.94×10^{-3}	120
0.800	0.195 3	0.004 3	0.764 5	6.28×10^{-4}	140
0.750	0.154 8	0.008 7	0.768 3	3.69×10^{-4}	130
0.700	0.171 7	0.005 3	0.808 3	1.8×10^{-4}	130
0.650	0.143 1	0.002 8	0.814 7	7.06×10^{-4}	130
0.600	0.130 0	0.003 4	0.833 2	9.6×10^{-4}	130

L	η_0	α_0	C_0	χ^2/DOF	NMCS (K)
40	0.294 2	0.011 3	0.747 2	1.63×10^{-4}	290
48	0.289 2	0.010 4	0.744 3	0.77×10^{-4}	290
60	0.280 2	0.006 7	0.743 6	4.02×10^{-4}	250
72	0.276 3	0.004 8	0.745 1	9.1×10^{-4}	250
84	0.265 3	0.003 4	0.736 2	6.6×10^{-4}	250
96	0.271 3	0.004 1	0.740 1	4.6×10^{-4}	250

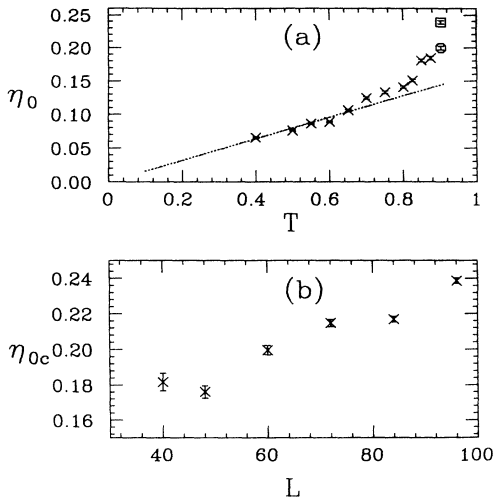

FIG. 3. (a) Results for $\eta_0(T)$ obtained from algebraic fits to $g_0(r)$ for $L=60$. The dotted line is the spin-wave results. (b) shows $\eta_{0c}(T=T_{BKT})$ vs L.

TABLE III. (Top) Gives the finite-size results for Υ^{o}_{BKT}, while (bottom) gives the corresponding results for $\Upsilon_{T_{U(1)}}$

L	$\Upsilon^o(T=T_{BKT})$	NMCS (K)
8	0.665 4(19)	200
16	0.645 5(34)	100
24	0.638 0(19)	200
32	0.627 9(33)	200
48	0.625 6(30)	290
60	0.622 5(24)	250
72	0.618 7(29)	250
84	0.618 1(28)	250
96	0.610 4(23)	250

L	$\Upsilon(T=T_{U(1)})$	NMCS (K)
8	0.436 1(34)	200
16	0.403 7(37)	200
24	0.376 2(43)	200
32	0.396 3(24)	290
48	0.356 5(48)	290
60	0.384 8(36)	250
72	0.385 0(31)	250
84	0.383 5(31)	250
96	0.378 0(38)	250

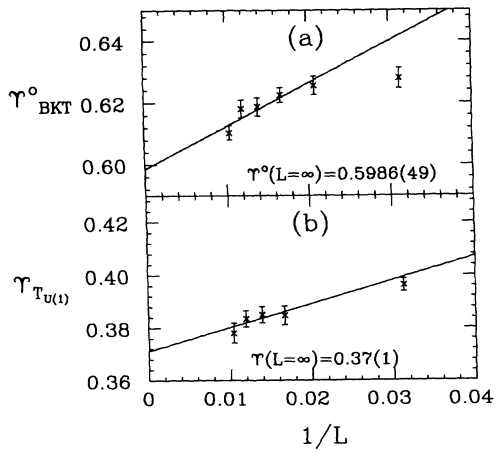

FIG. 4. (a) Finite-size analysis of $\Upsilon^{\circ}(T=T_{BKT})=\Upsilon^{\circ}_{T_{BKT}}$, with T_{BKT} obtained from the $g_0(r)$ analysis, as a function of $1/L$ for $L=96$, 84, 72, 60, 48, and 32. The straight line is a linear fit to the data, with the $L=\infty$ extrapolated value indicated. (b) The same as in (a) for $\Upsilon(T=T_{U(1)})=\Upsilon_{T_{U(1)}}$.

$$\Upsilon^{0}(T_{BKT})=0.5752(4)\,, \tag{26}$$

which is about 3% below the value in Eq. (25). Next, we considered the relationship between the exponent η_0 and the universal prediction for the jump in $\Upsilon^{0}(T_{BKT})$,[38] that is $\eta_0=k_B T_{BKT}/[2\pi\Upsilon^{0}(T_{BKT})]$. Before inserting the numbers it is important to stress the fact that the three quantities appearing in this equation were obtained from three different calculations. The critical temperature was calculated from the coherence length analysis in the high-temperature phase, $\Upsilon^{0}(T_{BKT})$ from a finite-size analysis at T_{BKT}, and the η_0 from a finite-size analysis of the algebraic correlation functions at T_{BKT}. Plugging in the numbers gives the result

$$\eta_0=0.2402(18)\,, \tag{27}$$

which indicates that the values of these quantities satisfy, within the errors, the universality relation for the jump in Υ^{0} at T_{BKT}.

In conclusion, we have shown in this section that our strategy yields reasonable quantitative estimates of the critical temperature, critical exponents and the magnitude of the jump of $\Upsilon^{0}(T_{BKT})$ in the *XYM*. It is reassuring that independent calculations lead to essentially the same quantitative results. Building from what we have learned in this section about the *XYM*, in the next section we proceed to apply the same logic and analysis to the study of the phase transition(s) in the FF*XYM*.

IV. CRITICAL PROPERTIES OF THE FULLY FRUSTRATED 2D *XY* MODEL

In this section we present the bulk of our thermodynamic and correlation function results for both the U(1) and Z_2 freedoms. We start by discussing the thermodynamic properties and then we move on to present our results for the correlation functions.

A. Thermodynamic properties

1. U(1) freedoms

We begin by discussing the helicity modulus $\Upsilon(T)$. Previous studies[4,39] of the FF*XYM* and the fully frustrated Coulomb gas[17] have indicated the possibility that the jump in $\Upsilon(T)$ may be different from the universal *XYM* result. To further shed light onto this problem we have studied $\Upsilon(T)$ as a function of temperature for different lattice sizes and carried out a finite-size analysis of $\Upsilon_{U(1)}=\Upsilon(T=T_{U(1)})$. Figure 5 shows the results in the temperature range $0.20<T<0.65$ obtained from runs for $L=8$, 16, 32 with 250 K MCS and $L=60$ with 200 K MCS. Notice that at low temperatures the finite-size effects are almost negligible, however, they become important in the critical region. The behavior for $L=32$ and 60 is about the same in the temperature region where Υ was calculated. To investigate the magnitude of the jump in Υ we proceed as in the *XYM* calculations. We performed a finite-size analysis of Υ at the critical temperature $T_{U(1)}=0.44$, found from a high-temperature analysis of the correlations, to be discussed later. The simulations were carried out in lattices of size $L=8$, 16, 24, 32, 48, 60, 72, 84, and 96 and the results are given in Table III (bottom). The behavior of $\Upsilon_{U(1)}$ as a function of $1/L$ is shown in Fig. 4(b) for $L=96$, 84, 72, 60, and 48. The value

$$\Upsilon_{U(1)}=0.37(1) \tag{28}$$

was estimated by extrapolating the data to an infinite lattice. This result suggests that for the lattice sizes and statistics of our simulations, the jump in the helicity modulus for the FF*XYM* is about 23% below the *XYM* result. The estimate $\Upsilon(T=T_{CG})=0.34(1)$ was obtained from MC simulations of the fully frustrated *Coulomb gas* on a square lattice[17] using the formula $\Upsilon=T_{CG}/[2\pi\epsilon_c T_{CG}]$ with the values $\epsilon_c^{-1}=0.63(3)$, and $T_{CG}=0.129(2)$. Here, ϵ_c is the value of the dielectric constant at T_{CG}. Thus, our extrapolated value for Υ_c and the one obtained from the Coulomb gas data differ by about 7%, which can be considered in reasonable agree-

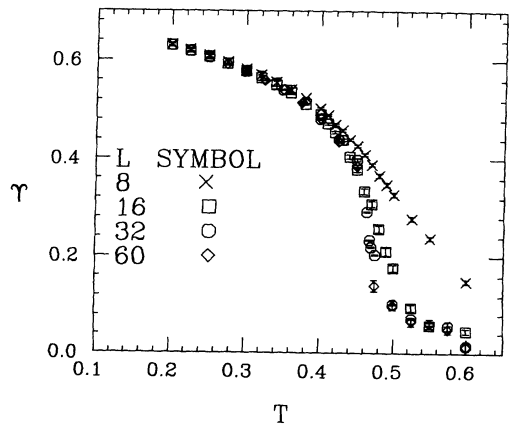

FIG. 5. Υ as a function of T for different L sizes. Note that the data for $L=32$ and 60 almost fall on top of each other, suggesting that the L dependence is almost negligible for $L\geq 32$.

ment. Note, however, that one cannot rule out the possibility of a smaller value of $\Upsilon_{T_{CG}}$ for larger lattices. Nonetheless, we do not believe that the trend would change significantly from the result given here. This result confirms previous suggestions[4,17] and gives support to Minnhagen's heuristic conjecture[39] about the difference between the jump of $\Upsilon_{T_{CG}}$ for the frustrated Coulomb gas in a square lattice as compared to the *XYM* universal jump.

It has also been suggested[14] that the transition in the FF*XYM* could be weakly first order. To check this possibility we looked at the histogram of the energy about $T_{U(1)}$ and found no evidence for the existence of two competing states. In previous MC simulations[4,6,7,14,15,17] it was found that the behavior of the maximum of the specific heat as a function of lattice size was consistent with a logarithmic divergence, favoring an Ising-like transition. However, MC simulations in larger lattices[20] suggest that it is very difficult to distinguish between a logarithmic or a power-law divergence. We have studied the specific heat and found no signature for a logarithmic divergence but we were unable to extract reliable exponents.

We have also studied the staggered magnetization M_{stagg} [Eq. (5)] due to the supercurrents circulating around the plaquettes as a function of temperature and lattice size. Figure 6 shows the behavior of M_{stagg} as a function of T for $L=16$ and 32. It is nonzero at low temperatures and drops sharply at about $T=0.42$. We note that finite-size effects are almost negligible for these lattice sizes. The behavior of M_{stagg} as a function of temperature suggests that it may be considered as an order parameter for the U(1) phase transition. Note, however, that the chirality is defined in terms of the direction of the circulating currents about the plaquettes and thus M_{stagg} can also be thought of as an order parameter for chirality.

2. Z_2 freedoms

We calculated the staggered chiral magnetization $\mathcal{M}_s$ defined in Eq. (7). However, $\mathcal{M}_s$ oscillates too irregularly between positive and negative values, thus it was more convenient instead to study[7] $\mathcal{M}_s^2$ and its fluctuations χ_s^2. These quantities are plotted as a function of temperature for $L=32$ and 60 in Figs. 7(a) and 7(b), respectively. $\mathcal{M}_s^2$ goes to unity at low temperatures and it decays sharply to zero close to the critical region. Note that χ_s^2 displays an asymmetric behavior close to $T_{Z_2}(\approx 0.42$ for $L=60)$, where it has a sharp maximum. This indicates that the critical exponents for χ_s^2 above and below T_{Z_2} should be different. For $T > T_{Z_2}$ we fitted the MC data to

$$M_s^2 \sim (\epsilon_{Z_2})^{2\beta}$$

and (29)

$$\chi_s^2 \sim (\epsilon_{Z_2})^{-2\gamma}$$

while for $T \le T_{Z_2}$ χ_s^2 was fitted to

$$\chi_s^2 \sim (-\epsilon_{Z_2})^{-2\gamma'} . \tag{30}$$

We extracted the critical exponents 2β, 2γ, and $2\gamma'$ by a straight-line fit to $\ln(\mathcal{M}_s^2)$ versus $\ln[\epsilon_{Z_2}(L)]$ and $\ln(\chi_s^2)$ versus $\ln[|\epsilon_{Z_2}(L)|]$ for temperatures within 10% from the estimated $T_{Z_2}(L)$. Here we used the notation $\epsilon_{Z_2}=(T-T_{Z_2})/T_{Z_2}(L)$, with $T_{Z_2}(L)$ the temperature at which $\mathcal{M}_s^2$ goes steeply to zero and χ_s^2 shows a maximum for a given L. The exponents obtained for the largest lattice were

$$2\beta = 0.1936(35) ,$$
$$2\gamma' = 1.025(79) , \tag{31}$$

and

$$2\gamma = 1.82(13) .$$

These exponents clearly differ from the corresponding 2D Ising model exponents $2\beta=\frac{1}{4}$, $2\gamma=2\gamma'=\frac{7}{2}$. We note that

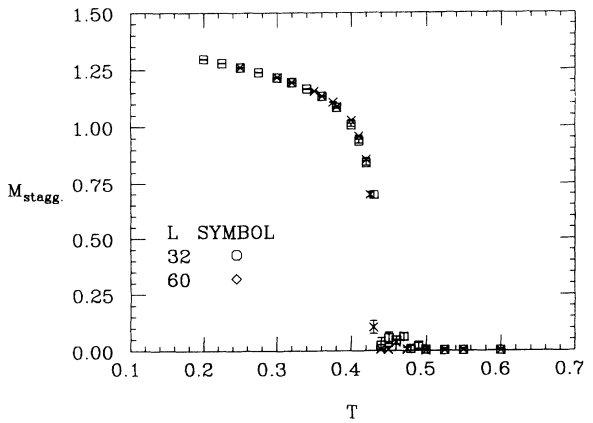

FIG. 6. Staggered magnetization due to the superconducting currents defined in Eq. (5) as a function of T for $L=32$ and 60. The falloff to zero occurs at about $T=0.42$.

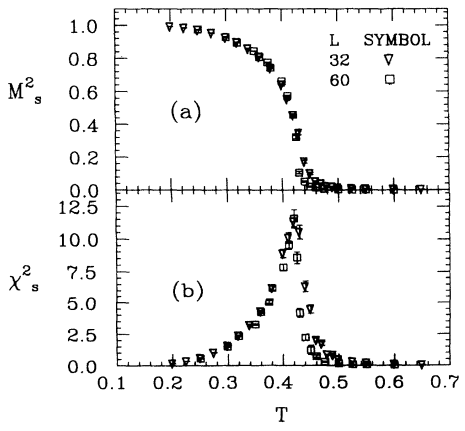

FIG. 7. Staggered chiral magnetization square M_s^2 (a) and susceptibility χ_s^2 (b) as a function of T for $L=32$ and 60. The results for both lattice sizes are essentially on top of each other. Note that $\mathcal{M}_s^2$ goes to zero at essentially the same T at which χ_s^2 has a maximum with $T_{Z_2}\approx 0.42$. Observe the asymmetric behavior of χ_s^2 about critical temperature.

our chiral order-parameter exponent does agree with the value $2\beta=0.20(2)$ obtained from MC transfer-matrix studies of the FF*XYM*.[25] The results for $L=16$, 32, and 60 are given in Table IV. Notice the consistency in the behavior of $\mathcal{M}_s^2$ which falls off to zero at about the same temperature where χ_s^2 has a maximum, indicating that the Z_2 phase transition takes place at $T_{Z_2}\approx 0.42$.

B. Correlation functions

1. U(1) correlations

In this subsection we discuss our MC results for the gauge-invariant phase correlation functions obtained from simulations in lattices from $L=16$ up to 240, with periodic boundary conditions. Some of these results have already been discussed in Ref. 22 and thus we will make reference to them here. To reduce finite-size effects the lattice sizes at each temperature were chosen such that $L/\xi\geq 5$. As we mentioned in Sec. III B, this criterion has proven to work well in the numerical calculations of correlation functions in the *XYM*. We showed in Ref. 22 that the zero-momentum phase correlation function $g_{\mathrm{U}(1)}(r)$ has an oscillatory behavior with period $\frac{1}{2}$, which comes from the Aharanov-Bohm phase factors discussed in Sec. II C.[3] At higher temperatures we found that the oscillatory behavior disappears, as one would expect. As the critical temperature is approached from above the oscillations increase in amplitude and saturate below $T_{\mathrm{U}(1)}$. This oscillatory behavior led us to separate the correlation functions into two components; one for the odd and one for the even lattice sites, with their corresponding coherence lengths ξ_o and ξ_e. The MC data for the zero-momentum correlation functions was fitted to the periodic version of the *ansatz* given in Eq. (16) for $T\geq T_{\mathrm{U}(1)}$. This procedure incorporates the periodic boundary conditions due to the finiteness of the lattice [Eq. (22)]. We carried out unconstrained nonlinear three-parameter fits to the data to obtain $\xi(T)$, $\eta(T)$, and the coefficient A for the odd and even correlation functions. We followed our *XYM* approach and fitted the MC data to the linear functions

$$\ln[g(r)]=\ln A+\ln[r^{-\eta}e^{-r/\xi}+(L-r)^{-\eta}e^{-(L-r)/\xi}]\ , \tag{32}$$

varying η until a minimum for χ^2 was reached. In Table I of Ref. 22 we gave the results for ξ_o and ξ_e as a function of temperature and lattice size, as well as the statistics of the runs. As one gets closer to the critical temperature from above, the coherence length increases exponentially and one needs longer simulations and larger lattices in order to get statistically reliable data. Furthermore, the fitting parameter $\eta(T)$ defined in Eq. (16) increases and oscillates rapidly, for both the odd and the even lattices so that an estimate of $\eta(T_{\mathrm{U}(1)})$ was not attempted. The same situation was encountered in the *XYM* as described in Sec. III B. We also found that as the temperature decreases, A_o decreases while A_e increases, both slowly. Far from the critical region we got reliable results for ξ_o and ξ_e using lattices of size $L\leq 60$. However, to obtain meaningful results as we got closer to the critical region, L was increased keeping the ratio $L/\xi\geq 5$. For instance, we had to increase the size up to $L=240$ for temperatures that were about 3 and 2% away from $T_{\mathrm{U}(1)}$. In contrast, in our *XYM* calculations the approach to T_{BKT} was only on the order of 10%. In Fig. 2 of Ref. 22 we showed the results for ξ_o. Similar results are obtained for ξ_e. We found that for the temperatures considered here $\xi_o<\xi_e$. In the determination of the critical exponents and the critical temperature it is crucial how one fits the data, as discussed in Ref. 46. We first tried a four-parameter unconstrained nonlinear fit to the MC data of BKT type [Eq. (17)] obtaining the results,

$$\nu_e=0.3133(57)$$

and

$$\nu_o=0.3005(6)\ , \tag{33}$$

which are close to $\frac{1}{3}$. We then fixed the values $\nu_e=\nu_o=\frac{1}{3}$, and carried out a three-parameter fit to the data for both lattices. The quality of the fits improved and hence we could surmise that the correct value of this exponent may indeed be $\frac{1}{3}$. The first column of Table II in Ref. 22 listed the results obtained from these fits together with their corresponding χ^2/DOF. For completeness we also carried out fits assuming $\nu=\frac{1}{2}$, the standard BKT value, and although the χ^2 function was smaller than when $\nu=\frac{1}{3}$, we found the differences too small to decide with absolute confidence from our data which exponent is the correct one. Nonetheless, as it will be seen below, we have other arguments, for example, the finite-size scaling analysis of the data, that yields better results when $\nu=\frac{1}{3}$, suggesting that this may very well be the correct value.

It should be stressed that doing nonlinear fits is a nontrivial matter since there is no guarantee that the values of the estimated parameters correspond to the absolute minimum of the χ^2 function. Therefore, one needs to check the results very carefully and oftentimes resort to different fitting procedures to cross-check the results. For instance, a good test to check the stability of the results is to reduce the dimension of the parameter space by fixing one of the parameters and carrying out the fitting procedure for the others. This process should be repeated[43–46] for a set of values of the parameter held fixed within an interval about the value which is supposed to yield the minimum to χ^2. In some instances it is worthwhile to use the value of more than one parameter, say two, to reduce the problem to a linear fit. For exam-

TABLE IV. Magnetic critical exponents for the Z_2 transition for $L=16$, 32, and 60. See text for definition of the parameters.

$M_s^2\sim(-\epsilon_{Z_2})^{2\beta}$ 2β	$\chi_s^2\sim(\epsilon_{Z_2})^{-2\gamma}$ 2γ	$\chi_s^2\sim(-\epsilon_{Z_2})^{-2\gamma'}$ $2\gamma'$	L
0.193 6(35)	1.82(13)	1.025(79)	60
0.205 5(27)	2.15(13)	1.029(63)	32
0.229 8(41)	1.69(15)	0.46(6)	16

ple, in the calculation of ν and $T_{U(1)}$ we carried out linear fits to

$$\ln(\xi)=\ln(A)+B(T-T_{U(1)})^{-\nu}, \tag{34}$$

with $\nu=\frac{1}{2}$ or $\frac{1}{3}$ while varying $T_{U(1)}$ about the value $T_{U(1)}=0.446$, obtained from the nonlinear fits. We found that sometimes these fits led to different values of the parameters A and B and also to different values for the minimum of the χ^2 function. However, the different values of $T_{U(1)}$ extracted from these fits were not significantly different. This uncertainty in the analysis must be due to the complicated topology of the parameter space and, although our calculations are very extensive, the number of points used in the fits with their corresponding statistical significance may not be sufficient to obtain a clear minimum for the χ^2 function.

Another possible source of problems relates to the size of the errors that weight each value of $\xi(T)$ in the fits. In our calculations most of the errors were on the order of 10^{-3} (see Table I of Ref. 22) and, because of the small number (12) of available data points we obtained relatively large values for the χ^2 function. This, in turn, led to small Q values (Q being the *goodness of fit*). In most cases we found $Q\leq 0.10$, suggesting that the data did not fit the model well. To sort out this problem we followed standard practice by setting $\sigma_i^2=1$ and carried out the fits again.[51] We found that by doing this the values of Q became larger than 90% in most cases, and the values of the fitted parameters remained basically the same but with slightly smaller errors. The values shown in Table II of Ref. 22 were, in fact, obtained following this type of analysis. One will need to have more points to improve the quality of the fits. To do this one needs to carry out calculations even closer to the critical point. One of the major problems in undertaking such a program is the lack of an efficient algorithm that could reduce effectively the critical slowing down. For the known algorithms that reduce the critical slowing down there has been the need to know in some detail their elementary excitations. In a sense this is equivalent to having to know the main features of the solution to the model before an appropriate algorithm can be tailored.

As an additional test of the reliability of the results for $T_{U(1)}$ and ν, we carried out a finite-size scaling analysis of the data for ξ_o and ξ_e. For a finite system, assuming periodic boundary conditions, the usual $T>T_{U(1)}$ finite-size scaling *ansatz* for a BKT transition is

$$\xi(T,L)\sim LF_{\xi}[L^{-1}\exp(B_{\xi}\epsilon^{-\nu})], \tag{35}$$

with F_{ξ} the scaling function, not known *a priori*, which must satisfy the conditions

$$F_{\xi}(x)=0 \quad \text{as } x\to 0,$$

$$F_{\xi}(x)<\infty \quad \text{as } x\to\infty .$$

The idea is to find the set of parameters B, ν, and $T_{U(1)}$ for which the data for different temperatures and lattice sizes fall onto one curve. Fixing $\nu=\frac{1}{3}$, we varied the values of B and $T_{U(1)}$ about their values obtained in the previous fits. We found that as we moved away from those values in the increasing or decreasing directions, the data became more scattered. However, very close to the values found from the previous fits the data fell very close to a unique curve. The values for which the data collapsed approximately onto the universal curve were

$$B_e=1.045, \quad B_o=0.999$$

and (36)

$$T^e_{U(1)}=0.440, \quad T^o_{U(1)}=0.442 .$$

These numbers are in rather good agreement with the values found in the previous fits. In the inset of Fig. 2 of Ref. 22 we showed the results of such analyses for the odd lattice. Similar results are obtained from the analysis of even lattices. We see that close to the critical region the points corresponding to lattices $L\leq 60$ are far from the universal curve. The equivalent finite-size scaling analysis fixing $\nu=\frac{1}{2}$ always led to a rapidly increasing curve suggesting that closer to the critical point it would diverge. This analysis provides further support in favor of $\nu=\frac{1}{3}$.

As in the XYM analysis, we also tested a power-law fit to the $\xi(T)$ data, and the results are given in the third column of Table II of Ref. 22. We find that the BKT and power-law fits are of comparable quality, as in the XYM case. Hence, one cannot be absolutely sure from this analysis alone which one of the two fits is the correct one. In trying to resolve this ambiguity we also calculated $g_{U(1)}(r)$ below $T_{U(1)}$, mostly for $L=60$. In fitting the corresponding data to an algebraic form we followed a procedure that parallels the one discussed in Sec. III B. The results of the analyses are presented in Table V (top) and (second section). In Fig. 8, we show the exponents $\eta_o(T)$ (□) and $\eta_e(T)$ (○) obtained from the algebraic fits to $g_{U(1)}(r)$. A careful look at the numbers indicates that the trend in $\eta(T)$ for both lattices is qualitatively similar to the one found in the XYM, but they are quantitatively different. The exponential fits to $g_{U(1)}(r)$ appear to yield better results with $\alpha\leq 10^{-2}$, and larger values for $\eta(T)$ than the ones obtained with an algebraic fit, see the results in Table VI (top) and (second section). Nonetheless, the values of α decreased as the lattice sizes increased, suggesting that at the asymptotic limit the leading contribution will mostly come from the algebraic part of the correlations. We also calculated η_e and η_o at the average critical temperature $T_{U(1)}\equiv\frac{1}{2}(T^o_{U(1)}+T^e_{U(1)})$ obtained from the high-temperature analyses for lattices with $L=32$, 40, 48, 60, 72, 84, and 96. The results from the finite-size analysis of the algebraic fits are summarized in Table V (third section) and (bottom), whereas we list the corresponding results for the exponential fits in Table VI (third section) and (bottom). The resulting values for η_e and η_o as a function of L are shown in the inset of Fig. 8. For comparison we also show η_0. Observe that η_o is systematically above η_e and that the behavior of these exponents as a function of L is qualitatively similar to those found in the XYM, e.g., the η's increased monotonically with L without appearing to saturate for the values considered. However, the η's do seem to reach a more asymptotic value for the FFXYM than for the XYM.

From the above analysis we extracted the results

$$\eta_o(T_{U(1)})=0.1955(3)$$

and (37)

$$\eta_e(T_{U(1)})=0.1875(3)\ .$$

On the other hand, we get

TABLE V. Results from algebraic fits to $g_{U(1)}(r)$, (top) odd and (second section) even lattices for $T<T_{U(1)}$ with $L=60$. Results of a finite-size analysis of the algebraic fits to $g_{U(1)}(r)$ for the odd (third section) and even (bottom) lattices at $T=T_{U(1)}$.

T	η_o	C_o	χ^2/DOF	NMCS (K)
0.4406	0.1666	0.478	2.08×10^{-2}	250
0.425	0.1355	0.5041	2.10×10^{-2}	70
0.400	0.1215	0.5433	1.13×10^{-2}	70
0.375	0.1095	0.5688	0.94×10^{-2}	70
0.350	0.0918	0.5799	1.55×10^{-2}	90
0.325	0.0770	0.5896	1.41×10^{-2}	100
0.300	0.0636	0.5964	2.22×10^{-2}	100
0.275	0.0674	0.6119	0.96×10^{-2}	100
0.250	0.0557	0.6247	1.78×10^{-2}	100
0.225	0.0489	0.6335	1.27×10^{-2}	100
0.200	0.0391	0.6386	2.31×10^{-2}	100

T	η_e	C_e	χ^2/DOF	NMCS (K)
0.4406	0.1535	0.6521	1.55×10^{-2}	250
0.425	0.1298	0.7011	1.19×10^{-2}	70
0.400	0.1186	0.7617	0.68×10^{-2}	70
0.375	0.1079	0.8005	0.59×10^{-2}	70
0.350	0.0887	0.8132	1.37×10^{-2}	90
0.325	0.0734	0.8261	1.28×10^{-2}	100
0.300	0.0616	0.8384	1.37×10^{-2}	100
0.275	0.0659	0.8721	1.00×10^{-2}	100
0.250	0.0538	0.8748	1.99×10^{-2}	100
0.225	0.0470	0.8915	1.24×10^{-2}	100
0.200	0.0381	0.9003	1.62×10^{-2}	100

L	η_o	C_o	χ^2/DOF	NMCS (K)
32	0.159	0.479	0.515×10^{-2}	290
40	0.169	0.486	0.651×10^{-2}	290
48	0.1599	0.475	1.60×10^{-2}	290
60	0.1666	0.478	2.08×10^{-2}	250
72	0.1808	0.489	1.80×10^{-2}	250
84	0.1721	0.4790	3.12×10^{-2}	250
96	0.1955	0.4950	1.77×10^{-2}	250

L	η_e	C_e	χ^2/DOF	NMCS (K)
32	0.138	0.6450	0.43×10^{-2}	290
40	0.1526	0.6661	0.52×10^{-2}	290
48	0.1431	0.6428	1.16×10^{-2}	290
60	0.1535	0.6521	1.55×10^{-2}	250
72	0.1708	0.6723	1.35×10^{-2}	250
84	0.1643	0.6599	2.19×10^{-2}	250
96	0.1875	0.6830	1.33×10^{-2}	250

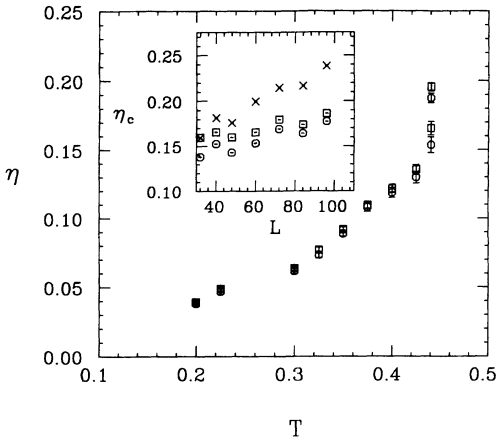

FIG. 8. Results for $\eta_o(T)$ (□) and $\eta_e(T)$ (○) obtained from algebraic fits to $g_{U(1)}(r)$ for $L=60$. The inset shows the results for the finite-size analysis for the critical exponents η_0 (□), η^e (○), and η^o (×), at criticality.

$$\eta_o(T_{U(1)})=0.2521(3)$$

and (38)

$$\eta_e(T_{U(1)})=0.2480(3)\ ,$$

assuming the exponential fits to the correlations. We note that in the algebraic fits the values of η_o and η_e are smaller than in the exponential case, as in the XYM analysis, and clearly $\eta\neq\eta_0$.

Again as in Sec. II C, we carried out a check of the universal jump relationship as applied to the average values of the even and odd lattice results. We found that the universal jump is indeed satisfied for our FFXYM results with the jump at $T_{U(1)}$ of

$$\Upsilon(T_{U(1)})=0.37(1)\ , \tag{39}$$

clearly different than the XYM universal jump. Apart from giving a strong consistency check of the set of results obtained by independent calculations this is a surprising finding, for there is no *a priori* reason why the universality results should be valid in the FFXYM, in particular, in light of the non-Ising and XY results from our study. In the XYM the universality of the jump in Υ is a consequence of an underlying universal RG result.[36–38] We can then just surmise that there may be an underlying RG argument that will lead to an understanding of the physical properties of the FFXYM.

2. Z_2 correlation functions

Let us now turn to the discussion of the correlation functions for the chiral degrees of freedom. Our study here will be less detailed than in the U(1) case, mainly concentrating on the temperature region above T_{Z_2}, although a few results for $T\leq T_{Z_2}$ will also be discussed. Prior information about the chiral critical exponents is available so that we can compare our results to them. The calculation of the zero-momentum chiral correlation functions defined in Eq. (15) is less demanding than in the $U(1)$ case since one expects that ξ_χ diverges algebraical-

ly. The analysis of $g_\chi(r)$ followed a similar logic to that of the U(1) study. The Fig. 9 inset shows $g_\chi(r)$ versus r above and below T_{Z_2}. The results for the coherence length $\xi_\chi(T)$ for different lattice sizes are given in Table VII. Figure 2 of Ref. 22 showed the results of a power-law fit of the data to

TABLE VI. Results from exponential fits to $g_{U(1)}(r)$ for the odd (top) and even (second section) lattices for $T<T_{U(1)}$ with $L=60$. Results from a finite-size analysis of exponential fits to $g_{U(1)}(r)$ for the odd (third section) and even (bottom) lattices at $T=T_{U(1)}$.

T	η_o	α_o	C_o	χ^2/DOF	NMCS (K)
0.4406	0.2623	0.0079	0.5424	2.27×10^{-5}	250
0.425	0.1886	0.0023	0.5477	2.2×10^{-4}	70
0.400	0.1552	0.00246	0.5696	4.4×10^{-4}	70
0.375	0.1345	0.00237	0.5867	4.2×10^{-4}	70
0.350	0.1189	0.00204	0.56010	1.2×10^{-4}	90
0.325	0.1052	0.00120	0.66135	0.81×10^{-4}	100
0.300	0.0929	0.00064	0.6231	8.3×10^{-4}	100
0.275	0.0809	0.00087	0.6292	5.8×10^{-4}	100
0.250	0.0744	0.001125	0.6381	0.91×10^{-4}	100
0.225	0.0695	0.00106	0.6446	0.91×10^{-4}	100
0.200	0.0540	0.00049	0.6500	0.76×10^{-4}	100

T	η_e	α_e	C_e	χ^2/DOF	NMCS (K)
0.4406	0.2577	0.0077	0.7599	4.18×10^{-5}	250
0.425	0.18767	0.0023	0.7724	3.94×10^{-4}	70
0.400	0.1571	0.00262	0.8073	5.43×10^{-4}	70
0.375	0.13646	0.00253	0.8320	4.69×10^{-4}	70
0.350	0.11980	0.00211	0.8510	1.31×10^{-4}	90
0.325	0.1079	0.00141	0.8712	8.69×10^{-4}	100
0.300	0.09569	0.00085	0.8849	8.83×10^{-4}	100
0.275	0.0824	0.00098	0.8919	6.42×10^{-4}	100
0.250	0.07521	0.00130	0.9035	0.68×10^{-4}	100
0.225	0.06506	0.00109	0.9123	0.61×10^{-4}	100
0.200	0.05433	0.00052	0.9198	1.13×10^{-4}	100

L	η_o	α_o	C_o	χ^2/DOF	NMCS (K)
32	0.2908	0.0151	0.5520	2.31×10^{-5}	290
40	0.2792	0.0117	0.5495	1.72×10^{-5}	290
48	0.2803	0.0112	0.5511	0.19×10^{-5}	290
60	0.2623	0.0079	0.5424	2.27×10^{-5}	250
72	0.2552	0.0057	0.5394	4.19×10^{-5}	250
84	0.2434	0.00473	0.5311	0.29×10^{-5}	250
96	0.2521	0.00366	0.5379	0.14×10^{-5}	250

L	η_e	α_e	A_e	χ^2/DOF	NMCS (K)
32	0.2944	0.0157	0.7812	4.9×10^{-5}	290
40	0.2915	0.0128	0.7898	2.82×10^{-5}	290
48	0.2744	0.0109	0.7710	0.32×10^{-5}	290
60	0.2577	0.0077	0.7599	4.18×10^{-5}	250
72	0.2506	0.0055	0.7555	6.23×10^{-5}	250
84	0.2375	0.00448	0.7418	25.0×10^{-5}	250
96	0.2480	0.00351	0.7539	20.0×10^{-5}	250

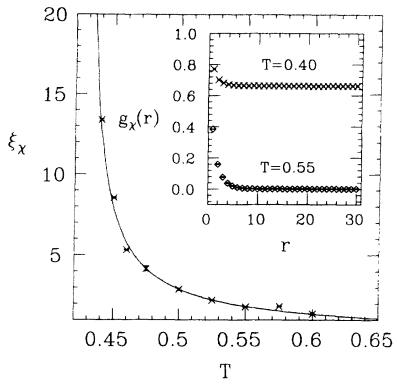

FIG. 9. Data for the chiral coherence length $\xi_\chi(T)$ (×) calculated from $g_\chi(r)$. The solid line is the fit to the form given in Eq. (20). The inset shows $g_\chi(r)$ as a function of r for temperatures above and below T_{Z_2}.

$$\xi_\chi \sim (\epsilon_{Z_2})^{-\nu_\chi} . \tag{40}$$

We also found that inclusion of the errors of $g_\chi(r)$ in the fits yielded results with rather low confidence levels ($Q<0.10$), as in the analysis of $g_{U(1)}(r)$. Again we followed standard procedure by assigning the same weight to each data point, with the resulting Q values in most cases above 0.90, while the fitted parameters remained essentially the same. In the ξ_χ case the errors in the fitting parameters became smaller after normalization of the errors in the $g_\chi(r)$ data points. It is difficult, however, to be absolutely sure that the values of the parameters found correspond to the absolute minimum of the χ^2 function, as happened in the U(1) case. Therefore, in addition to the nonlinear three-parameter fits, we also fitted the data to the linear function

$$\ln(\xi_\chi)=\ln(A_\chi)-\nu_\chi \ln(T-T_{Z_2}) . \tag{41}$$

Using a least-squares fit and varying the T_{Z_2} values about 0.42 we found

$$A_\chi=0.33(2) \quad \text{and} \quad \nu_\chi=0.80(1) \quad \text{for} \quad T_{Z_2}=0.430 , \tag{42}$$

with $\chi^2=3.99\times10^{-3}$. We also performed least-squares fits of the data to the straight line

TABLE VII. Results for $\xi_\chi(T)$ obtained from $g_\chi(r)$ at different temperatures and lattice sizes.

T	L	ξ_χ	NMCS (K)	L	ξ_χ	NMCS (K)
0.600	32	1.552(53)	160	60	1.392(18)	140
0.575	32	1.7579(62)	160	60	1.835(27)	140
0.550	32	2.1278(26)	160	60	1.8092(30)	140
0.525	32	2.7324(12)	160	60	2.229(15)	140
0.500	32	5.984(14)	160	60	2.8913(70)	140
0.475	60	4.15(16)	140			
0.460	60	5.625(19)	150	72	5.332(20)	150
0.450	60	8.168(37)	150	72	8.547(30)	150
0.440	60	24.51(1.69)	150	72	13.693(62)	240
0.440	96	13.405(47)	220			

$$\xi_\chi^{-1/\nu_\chi} = \tilde{A}_\chi T + b_\chi \ , \tag{43}$$

for fixed values of ν_χ with $\tilde{A}_\chi = A_\chi^{-1/\nu_\chi}$ and $b_\chi = A_\chi^{-1/\nu_\chi} T_{Z_2}$. Remarkably, the results obtained were

$$A_\chi = 0.36(3) \text{ and } T_{Z_2} = 0.432(9) \text{ for } \nu_\chi = 0.760 \ , \tag{44}$$

with $\chi^2 = 9.7 \times 10^{-2}$. Note that the results in Eq. (44) are close to those in Eq. (42), with essentially the same T_{Z_2}. In Table VIII we give the values of the parameters extracted from the nonlinear fit. Our result for ν_χ agrees quite well with recent finite-size scaling analysis[20] that gave $\nu_\chi = 0.85(3)$, as well as with the MC transfer-matrix calculations.[25] The advantage of the finite-size scaling analysis is that ν_χ was obtained from a one-parameter fit without needing a precise value for T_{Z_2}, as in our analysis. Therefore, it appears that the ν_χ and T_{Z_2} values obtained here from the nonlinear fits may in fact be very close to the correct ones. It is important to emphasize that the T_{Z_2} found here is consistent with the temperature at which $\mathcal{M}_s^2$ fell to zero, and χ_s^2 displayed a sharp maximum.

In summary, our numerical analysis of the chiral degrees of freedom led to the critical exponents

$$\begin{aligned} 2\beta &= 0.1936(35) \ , \\ 2\gamma' &= 1.025(79) \ , \\ 2\gamma &= 1.82(13) \ , \end{aligned} \tag{45}$$

and

$$\nu_\chi = 0.875(35) \ .$$

These results strongly indicate that the Z_2 phase transition is not an Ising-like transition as had been suspected from previous thermodynamics studies of this model. The results for β and ν agree with previous calculations. If one believes that thermodynamic scaling relations should be valid then one should get a different value for γ and $\gamma = \gamma'$. There is a possibility that since we have been forced to calculate χ^2 rather than χ the results listed here are correct for χ^2 but not for χ itself.[52] Note that in our calculations the difference between T_{Z_2} and $T_{U(1)}$ is about 7%, which may not be considered as different within the size of our estimated errors. Equivalently, one cannot rule out the possibility that in improved numerical simulations and closer to the critical point this difference may disappear.

TABLE VIII. Exponent ν_χ and critical temperature T_{Z_2} obtained from nonlinear fits to a power-law divergence.

$\xi_\chi = A_\chi \epsilon_{Z_2}^{-\nu_\chi}$
$A_\chi = 0.292$
$T_{Z_2} = 0.427$
$\nu_\chi = 0.875$
$\chi^2/\text{DOF} = 0.0974$

V. CONCLUSIONS AND OUTLOOK

In this paper we have presented results from extensive MC calculations of the FF*XY*M. We have explicitly analyzed the separate contributions from the U(1) and Z_2 freedoms. We have extracted the U(1) and Z_2 critical exponents from direct calculations of their corresponding correlation functions and selected thermodynamic properties. We found compelling quantitative evidence that the U(1) and Z_2 critical exponents are clearly different from those of the usual 2D *XY* and Ising models. We have tested our results using several consistency checks. Our result for the Z_2 correlation length exponent ν_χ is essentially the same as the one obtained from other independent numerical calculations.[20,25] There are no previous calculations of the U(1) exponents to with which to compare our results. However, a reanalysis of the experimental data leads to an η exponent that is clearly different from the *XY*M result and that agrees reasonably well with the one found in our calculations.

Our result strongly suggest nontrivial critical behavior in the FF*XY*M, in which the U(1) and Z_2 freedoms are coupled in a way so as to yield critical exponents. We leave for the future the question of producing the physical understanding of the results presented in this paper, in particular the apparent relation between the U(1) results, $\eta_0^{-1}(f=0)=4$, $\nu_0^{-1}(f=0)=2$, and our values $\eta^{-1}(f=\frac{1}{2})=\eta_0^{-1}(f=0)+1$ and $\nu^{-1}(f=\frac{1}{2})=\nu_0^{-1}(f=0)+1$, together with the validity of a universal jump for the $f=\frac{1}{2}$ helicity modulus.

In spite of the extensive calculations and detailed analyses carried out in this paper, improved MC simulations of this system need to be done. More data at temperatures closer to the critical point are required to be able to obtain more accurate estimates of the critical exponents and critical temperatures. As noted above, among the major limitation in this program is the lack of a MC algorithm that could effectively minimize the critical slowing down. Another important limitation is that calculations of correlation functions near criticality require ever larger lattices which sharply increases the computer power requirements.

ACKNOWLEDGMENTS

We thank R. Gupta and H. van der Zant for illuminating conversations. One of us (J.V.J.) thanks Professor J. E. van Himbergen for his careful reading of this paper and for his kind hospitality at the Institute for Theoretical Physics in the University of Utrecht, where this paper was completed. This work was supported in part by NSF Grant Nos. DMR-9211339, INT-91-18193, the NSF Pittsburgh supercomputing center under Grant No. PHY88081P, the Northeastern University Research and Development Fund, and the Dutch Organization for Fundamental Research. The work of G.R.S. was also partially supported by CONACYT, México, by DGAPA-UNAM Project No. IN102291, and by NSF-CONACYT Grant No. G001-1720/001328.

[1]J. Villain, J. Phys. C **10**, 1771 (1977); **10**, 4793 (1977).
[2]E. Fradkin, B. A. Huberman, and S. Shenker, Phys. Rev. B **18**, 4789 (1978).
[3]J. V. José, Phys. Rev. B **20**, 2167 (1979).
[4]S. Teitel and C. Jayaprakash, Phys. Rev. B **27**, 598 (1983); Phys. Rev. Lett. **51**, 1999 (1983).
[5]W. Y. Shih and D. Stroud, Phys. Rev. B **28**, 6575 (1983); **30**, 6774 (1984).
[6]D. H. Lee, J. D. Joannopoulos, J. W. Negele, and D. P. Landau, Phys. Rev. Lett. **52**, 433 (1984); Phys. Rev. B **33**, 450 (1986).
[7]S. Miyashita and H. Shiba, J. Phys. Soc. Jpn. **53**, 1145 (1984).
[8]M. Y. Choi and S. Doniach, Phys. Rev. B **31**, 4516 (1985).
[9]Y. M. Choi and D. Stroud, Phys. Rev. B **32**, 5773 (1985); **35**, 7109 (1987).
[10]M. Yosefin and E. Domany, Phys. Rev. B **32**, 1778 (1985).
[11]T. C. Halsey, Phys. Rev. Lett. **55**, 1018 (1985); Phys. Rev. B **31**, 5728 (1985); J. Phys. C **18**, 247 (1985); S. E. Korshunov, J. Stat. Phys. **43**, 17 (1986); S. K. Korshunov, *ibid.* **43**, 1 (1986).
[12]E. Granato and J. M. Kosterlitz J. Phys. C **19**, L59 (1986); Phys. Rev. B **33**, 4767 (1986).
[13]J. E. van Himbergen, Phys. Rev. B **33**, 7857 (1986).
[14]B. Berge, H. T. Diep, A. Ghazali, and P. Lallemand, Phys. Rev. B **34**, 3177 (1986).
[15]J. M. Thijssen and H. J. F. Knops, Phys. Rev. B **37**, 7738 (1988).
[16]H. Eikmans, J. E. van Himbergen, H. J. Knops, and J. M. Thijssen, Phys. Rev. B **39**, 11 759 (1989).
[17]G. Grest, Phys. Rev. B **39**, 9267 (1989).
[18]J. M. Thijssen and H. J. F. Knops, Phys. Rev. B **42**, 2438 (1990).
[19]E. Granato, J. M. Kosterlitz, J. Lee, and M. Nightingale, Phys. Rev. Lett. **66**, 1090 (1991).
[20]J. Lee, J. M. Kosterlitz, and E. Granato, Phys. Rev. B **44**, 4819 (1991).
[21]J. R. Lee and S. Teitel, Phys. Rev. B **46**, 3247 (1992).
[22]G. Ramírez-Santiago, and J. V. José, Phys. Rev. Lett. **68**, 1224 (1992).
[23]A. Vallat and H. Beck, Phys. Rev. Lett. **68**, 3096 (1992).
[24]Jong Rim Lee, Phys. Rev. B **49**, 3317 (1994).
[25]E. Granato and M. P. Nightingale, Phys. Rev. B **48**, 7438 (1993).
[26]D. Kimhi, Fl. Leyvraz, and D. Ariosa, Phys. Rev. B **29**, 1487 (1984).
[27]Ch. Leeman, Ph. Lerch, G. A. Racine, and P. Martinoli, Phys. Rev. Lett. **56**, 1291 (1986).
[28]P. Martinoli, Ph. Lerch, Ch. Leeman, and H. Beck, Proceedings of the 18th International Conference on Low Temperature Physics, Kyoto, 1987 [Jpn. J. Appl. Phys. **26**, Supplement 263 (1987)].
[29]B. J. Van Wees, H. S. J. van der Zant, and J. E. Mooij, Phys. Rev. B **35**, 7291 (1987).
[30]H. S. J. van der Zant, H. A. Rijken, and J. E. Mooij, Jpn. J. Phys. **26**, Suppl. 263, 1994 (1987).
[31]J. P. Carini, Phys. Rev. B **38**, 63 (1988).
[32]H. S. J. van der Zant, H. A. Rijken, and J. E. Mooij, J. Low Temp. Phys. **79**, 289 (1990).
[33]B. Pannetier, J. Chaussy, and R. Rammal, J. Phys. (Paris) **44**, L1853 (1983).
[34]B. Pannetier, J. Chaussy, R. Rammal, and C. Villagier, Phys. Rev. Lett. **53**, 1845 (1984).
[35]V. L. Berezinskii, Zh. Eksp. Teor. Fiz. **61**, 1144 (1971) [Sov. Phys. JETP **32**, 493 (1971)].
[36]J. M. Kosterlitz and D. J. Thouless, J. Phys. C **6**, 1181 (1973); J. M. Kosterlitz, *ibid.* **7**, 1046 (1974).
[37]J. V. José, L. P. Kadanoff, S. Kirkpatrick, and D. R. Nelson, Phys. Rev. B **16**, 1217 (1977).
[38]D. R. Nelson and J. M. Kosterlitz, Phys. Rev. Lett. **39**, 1201 (1977).
[39]P. Minnhagen, Phys. Rev. Lett. **54**, 2351 (1985); Phys. Rev. B **32**, 7548 (1985).
[40]A. F. Hebard and A. T. Fiory, Phys. Rev. Lett. **50**, 1603 (1983); A. T. Fiory and A. F. Hebard, Phys. Rev. B **28**, 5075 (1983).
[41]M. Tinkham, D. W. Abraham, and C. J. Lobb, Phys. Rev. B **28**, 6578 (1983).
[42]R. A. Webb, R. F. Voss, G. Grinstein, and P. M. Horn, Phys. Rev. Lett. **51**, 690 (1983).
[43]R. Gupta, J. DeLapp, G. Betrouni, G. C. Fox, C. F. Baillie, and J. Apostolakis, Phys. Rev. Lett. **61**, 1996 (1988).
[44]U. Wolf, Nucl. Phys. **B322**, 759 (1989).
[45]R. G. Edwards, J. Goodman, and A. D. Sokal, Nucl. Phys. **B354**, 289 (1991).
[46]R. Gupta and C. F. Baillie, Phys. Rev. B **45**, 2883 (1992).
[47]See also J. F. Fernández, M. F. Ferreira, and J. Stankiewicz, Phys. Rev. B **34**, 292 (1986).
[48]J. V. José, G. Ramírez-Santiago and H. S. J. van der Zant, Physica B+C (to be published).
[49]A. L. Scheinine, Phys. Rev. B **39**, 9368 (1989).
[50]D. B. Nicolaides, J. Phys. A **24**, L231 (1991).
[51]W. Press *et al.*, *Numerical Recipes* (Cambridge University Press, Cambridge, 1986).
[52]Y. M. M. Knops, H. Knops, and J. Blote (private communication).